JOURNAL OF CATALYSIS 27, 246–265 (1972)

Chemisorption of Hydrogen on Iron

ESTEBAN CHORNET* AND ROBERT W. COUGHLIN

Center for Surface and Coatings Research, and Chemical Engineering Department, Lehigh University, Bethlehem, Pennsylvania 18015

Received February 15, 1972

The flash desorption technique has been used to study adsorption and desorption of hydrogen on very clean, reproducible surfaces of polycrystalline iron. Preparation of the surfaces was achieved by extensive outgassing *in vacuo*, followed by hydrogen reduction and finally by argon ion bombardment and annealing in ultrahigh vacuum.

The experimental results strongly suggest the presence of a single phase of chemisorbed hydrogen atoms at 298°K, which recombine upon desorption following a second order rate equation. For the clean iron surface, the activation energy for desorption is about 20.3 kcal mole^{-1}, and this energy remains nearly constant up to a surface coverage of about 0.2×10^{15} H-atoms cm^{-2}, decreasing thereafter with coverage. As surface coverage changes, both the preexponential factor of the desorption kinetic rate constant and the activation energy change, and, furthermore, they display the usual "compensation effect" interdependence.

Equilibrium data for the iron–hydrogen system, indicate that the adsorbed species is mobile, behaving as an ideal two-dimensional gas up to a coverage of 0.2×10^{15} H-atoms cm^{-2}. At higher adsorbed amounts, lateral interactions between adsorbed species cause a departure from ideality.

The initial rates of adsorption of hydrogen are consistent with an activated complex that requires about 0.5 kcal mole^{-1} for its formation.

I. Introduction

In the usual application of flash desorption or decomposition, the substrate (a filament, disc or slab) is ordinarily cleaned by heating in ultrahigh vacuum (*1*). High-melting point metals are used to permit thermal evaporation of the surface oxide and decarburization of the sample (with O_2, commonly) so that very pure surfaces can be obtained for adsorption studies. Many investigations have made use of this technique for studying hydrogen chemisorption on filaments (*2*) of tungsten, molybdenum, iridium and rhodium, and on oriented single crystals of tungsten (*3*). Extensions of the technique to lower-melting point metals, in which a stable oxide is present, have been carried out by Lapujoulade (*4*) and Gasser, Roberts and Stevens (*5*) in studies of the hydrogen–nickel system. The latter authors modified the cleaning procedure by reducing the stable surface oxide with hydrogen. In the work reported herein we describe how the technique can be improved by using argon ion bombardment and annealing *in vacuo* to clean the surface of the metal filament.

The importance of the reaction of hydrogen with iron and the scarce information concerning the kinetic parameters of the reaction at the clean surface have, in part, motivated this study. Although considerable progress has been made in the understanding of hydrogen chemisorption at metal surfaces (*6*) most of the recent such work on iron (*7*) has involved primarily calorimetric studies and conductivity measurements on evaporated films. A strong dependence of the adsorption heat upon adsorbed amount has been observed, and the possible existence of several kinds of adsorbed species, has been hypothesized from these results.

In the present study we have investigated the adsorption and desorption of hydrogen

* Faculté des Sciences Appliquées, Université de Sherbrooke, Québec, Canada.

on iron; the dependence of the respective rates on adsorbed amount, and the adsorption equilibria at low surface coverages.

II. Experimental Methods

A. Apparatus

A schematic representation of the apparatus is shown in Fig. 1. The cryosorbent pump was connected to the system through a Varian 1.5 in. bakeable valve for initial pumpdown to about 10^{-4} Torr. Lower pressures were then achieved using a 50 liter sec^{-1} Varian Vac Ion pump. A dynamic vacuum of $2\text{–}3 \times 10^{-10}$ Torr was readily attained after baking out and degassing the entire system which consisted of the metal parts, the gauge (IG), the ion bombardment cell, the quadrupole residual gas analyzer (QRGA) and the specimen. The pumping system was connected to the adsorption cell through a Granville-Phillips type L valve which could seal the cell when static measurements were made. The cell itself was a 250 ml. Pyrex bulb with several openings for the pressure sensors (with thoriated filaments) and the gas admission lines. The system was provided with Pyrex-Kovar glass-to-metal seal adaptors and type 309 stainless steel bellows at strategic locations. The QRGA could be isolated from the rest of the measuring system by a magnetically operated glass ball valve. The geometric volume of the cell was about 1.3 liters. The approach of Liang (*8*) was used to account for temperature nonuniformities within the volume of the apparatus.

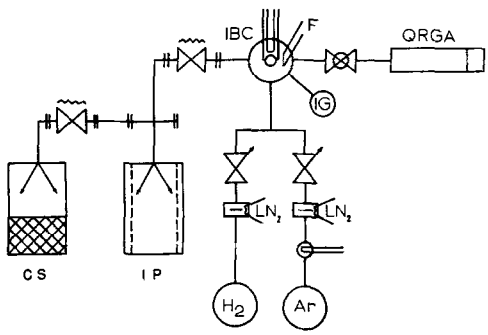

Fig. 1. Block diagram of the UHV apparatus for flash filament measurements. The pumping system is comprised of a 50 liter sec^{-1} Varian Vac Ion pump (IP) and a cryosorbent pump (CS) using Linde molecular sieve 13X; the measuring cell contains the ion bombardment unit (IBC); measuring sensors are a Granville-Phillips ion gauge (IG) and a Varian quadrupole residual gas analyzer (QRGA) separated from the cell by a glass ball-to-socket valve. The bellow valves are Granville-Phillips type L and Varian 1.5 in. bakeable valve (adjacent to cryosorbent). Throttling valves are Granville-Phillips variable leak type.

The arrangement of the interior of the cell depicted in Fig. 2, shows the ion bombardment unit. A cylindrical molybdenum grid, taken from an ionization gauge, was located in the center of the cell. A coiled tungsten wire (6 mil) acted as a cathode and the specimen hung in U-shape at 90° from a line passing from the emitter through the center of the grid. The specimen-grid distance was 3 to 5 mm. Pyrex-coated tungsten feedthroughs supported the different internal parts of the bombardment unit.

B. Sample Preparation

The substrates were very pure, cold-drawn wires (4 or 5 mil in diameter) of iron obtained from Materials Research Corp. which were spot welded to the feed-through holder. Good contact between the substrate wire and the tungsten was facilitated by using a small piece of nickel as intermediate. These specimens, about 12 cm long, were chemically polished by a solution of 5% H_2F_2 in 95% H_2O_2 for several seconds fol-

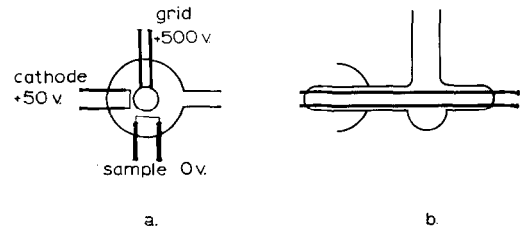

Fig. 2a. Horizontal cross-sectional view of the ion bombardment cell. The sample is spot-welded to the tip of the thick Pyrex-coated tungsten leads, and sealed to the glass holder. The cathode is a coiled tungsten filament which acts as an emitter of electrons. The molybdenum grid is cylindrically coiled and rests at the center of the cell. (b) Sample holder allowing conduction cooling at liquid nitrogen temperatures. The coolant is poured in from the top, and the holder is mounted at 30° inclination, thus facilitating a permanent liquid nitrogen contact at the tip of the feed-through.

lowed by a methanol and a distilled water rinse. After mounting and sealing the wires into the cell the system was evacuated using the cryosorbent and the Vac Ion pump. When 10^{-6} to 10^{-7} Torr was reached, the system was slowly heated to 400°C and held at this temperature for 12–14 hr. With the system still hot, all the metallic parts were carefully degassed. This step was followed by an initial heating (up to about 900°C) to outgas the sample which invariably resulted in a considerable pressure burst. After this operation, a second bakeout–degassing cycle was started. Twenty-four hours later, a dynamic vacuum of 3×10^{-10} Torr was reached with the specimen cold. The sample was then held at about 850°C (below the transition temperature of α-iron) for 30–48 hr, until a vacuum of 5×10^{-10} Torr could be achieved with the specimen hot.

After outgassing as described above, the specimens were still presumably covered by oxides and, therefore, were further treated by argon ion bombardment, using a procedure similar to that of Farnsworth *et al.* (*9*). During bombardment, in some cases, further annealing also took place as the specimen temperatures varied between 400 and 600°C, although some bombardments were conducted at room temperature. Aside from removing the oxide layer (the principal objective), the bombarding ions also penetrate the surface of the metal and lodge in the lattice, thereby creating defects. Upon subsequent heating, a complex dependence of the gas released upon temperature suggested the possible location of imbedded argon atoms in preferential positions near the surface of the metal. This behavior has been reported in detail elsewhere (*10*).

The ion bombardment was carried out at the potentials indicated in Fig. 2, and at 5 to 10 min intervals with an ion current density of about 100 μA cm^{-2} and argon pressure of $2\text{–}3 \times 10^{-3}$ Torr. After this, the argon was pumped out and the specimen was annealed for 10 to 15 min at 850°C by resistance heating. Almost invariably, an effective bombarding time of several hours was necessary before reproducible hydrogen adsorption was observed. In order to shorten this cleaning period we introduced a hydrogen reduction and decarburization step of 16–24 hr at 10^{-4} Torr, prior to the bombardment sequence. With this treatment, the entire bombardment procedure was reduced to an average of 2 hr. The criterion for cleanliness was to observe the amount of hydrogen adsorbed as a function of the number of ion bombardment cycles. When new cycles did not appreciably increase the total amount absorbed, it was concluded that a reproducible and clean surface had been achieved. The results were cross-checked by multiple tests with two different samples.

C. Gases

Argon (AirCo Assayed Reagent) was purified over a titanium getter and by passage through a freezing trap.

Hydrogen (AirCo Assayed Reagent) was purified by passage through a freezing trap.

D. Flash Desorption Experiments

Quantitative information was obtained by means of the flash filament technique (*1*), which is briefly summarized as follows: with the wire specimen held at about 800°C a flux of gas molecules is established in the measuring cell by adjusting the variable inlet leak valve and the outlet valve (Valve L). When steady-state flow is obtained, the electric current is then switched off causing the specimen to cool to room temperature within 2–3 min. Adsorption proceeds then at a rate dictated by the kinetics of the process. After a certain adsorption time, the current again is switched on through the wire, thereby heating the sample to a preselected maximum temperature, within a few seconds, during which desorption occurs. Pressure and filament resistance (from which temperature can be computed) are monitored as functions of time during the adsorption and desorption processes.

A material balance equation written for the experimental chamber enables computation of the amounts adsorbed or desorbed from the pressure variations and the characteristic constants of the vacuum system. During the few seconds duration of the desorption cycle, a unique effective pumping constant of the system can be calculated from the descending side of the desorption

peaks (pressure vs time). This approach was not used for the adsorption cycle (which requires a time interval of the order of minutes as opposed to seconds for the desorption) since, in this case, the effect of the walls, covered by the sputtered film produced during the bombardment, could not be approximated as a simple first order process. The results presented below are based on the analysis of the desorption peaks. Details of the calculations can be found in (*11*).

Kinetic information can be obtained from a formulation based on the Arrhenius equation:

$$-\frac{dn}{dt} = An^{\alpha}e^{-E_d/RT} \qquad (1)$$

where n the amount adsorbed at time t (molecules cm^{-2})

A the frequency (or preexponential) factor

α the reaction order

E_d the activation energy for desorption.

Since the temperature–resistance characteristics of the filament are rather complex, a numerical treatment similar to that of Degras (*12*) was developed in order to calculate the kinetic parameters α, E_d and A using a CDC 6400 computer.

III. Results

A. Adsorption at Various Stages of the Cleaning Procedure

The effects of cleaning and other treatments are shown in Fig. 3. One cleaning cycle consisted of one ion bombardment and one annealing period of 10–15 min at 800°C, as described above. The original surface, although extensively annealed and degassed, did not appreciably adsorb hydrogen. Even after 6 cleaning cycles and a reduction–decarburization period of 16 hr (stage 2 in Fig. 3), the amount adsorbed remained low (less than half the saturation value).

B. Rates of Desorption

1. Number of adsorbed phases at 298°C. Only one distinct hydrogen peak appears on a typical pressure versus time re-

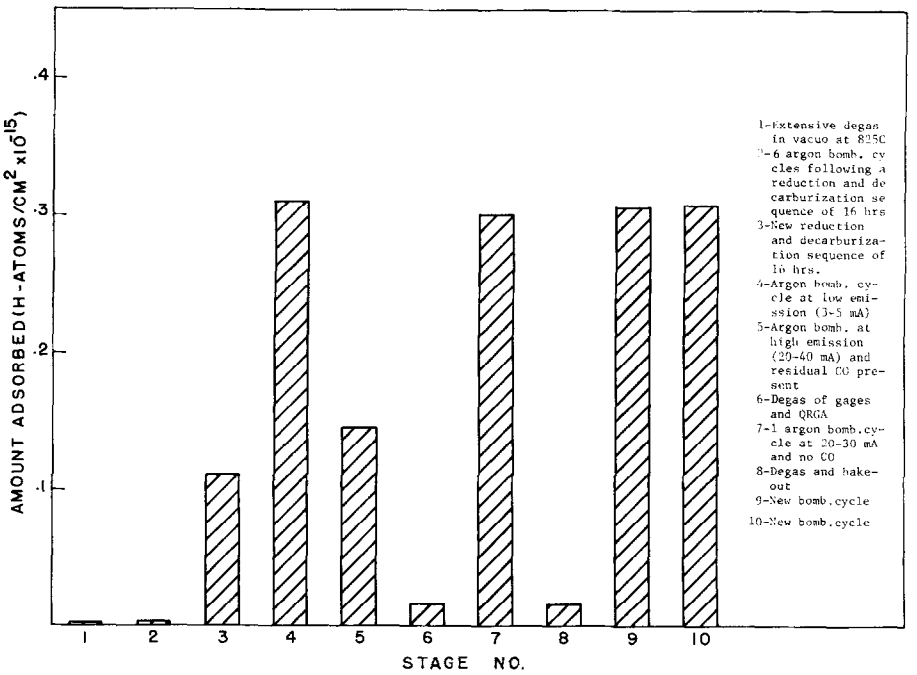

FIG. 3. Adsorption of hydrogen on iron at 298°K and 10^{-7} Torr, at various stages of the cleaning procedure.

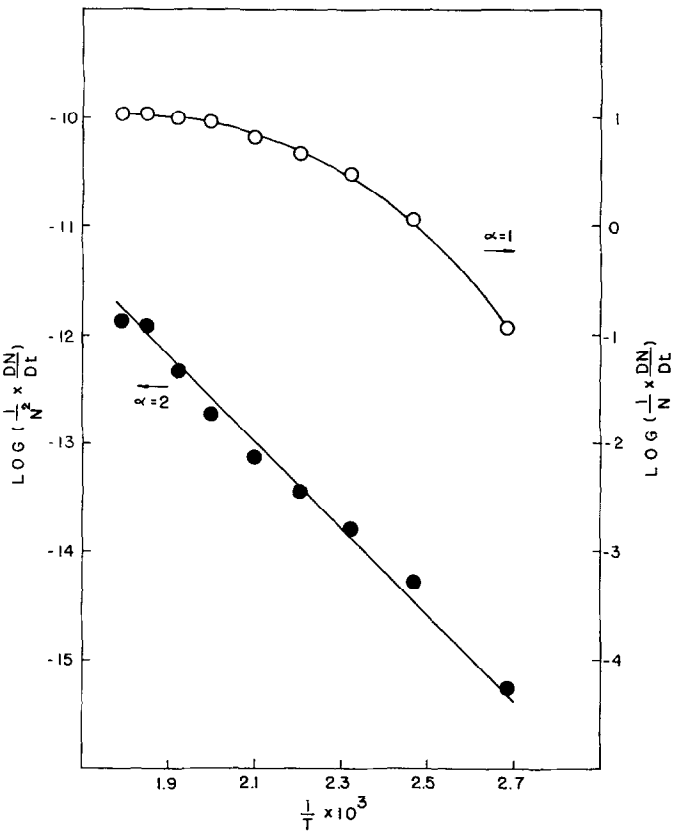

FIG. 4. Plots of $\log[(1/N^{\alpha})(dN/dt)]$ against $1/T$ for the desorption of hydrogen from iron. Initial coverage, 0.224×10^{15} H-atoms cm^{-2}.

cording, and this behavior was observed for a wide range of heating schedules and pumping speeds. At high exposure times (>20 min) a second hydrogen peak starts developing after desorption of the first one is complete. No quantitative estimate of this second peak was possible due to its small intensity.

2. Reaction order. Figure 4 shows plots of $\log[-(1/n^{\alpha})(dn/dt)]$ against $1/T$ at identical initial coverages for $\alpha = 1$ and $\alpha = 2$. It can be concluded from the linearity of the data for $\alpha = 2$ that the desorption process is a second order reaction. This second order process can be interpreted as involving the collision of two ad-atoms to form an activated complex intermediate in the desorption process.

3. Energies of activation and preexponential factor. The energies obtained from the Arrhenius plots assuming second order kinetics for desorption, as illustrated in Fig. 4, represent average activation energies for the desorption of the initial adsorbed population. Figure 5 shows these activation energies as a function of adsorbed amount. These energies appear to be relatively constant for low coverages, up to about 0.2×10^{15} H-atoms cm^{-2} whereupon this activation energy decreases gradually with additional adsorbed amounts. If there were not activation energy for adsorption, the activation energies calculated for desorption would also represent the adsorption heats.

Figure 6 shows the variation of the preexponential factor A with the activation energy E_d. The plot suggests a logarithmic relationship:

$$\ln A = \ln A_0 + \frac{E_d}{RT_m}, \qquad (2)$$

where A_0 is a constant and T_m is the iso-

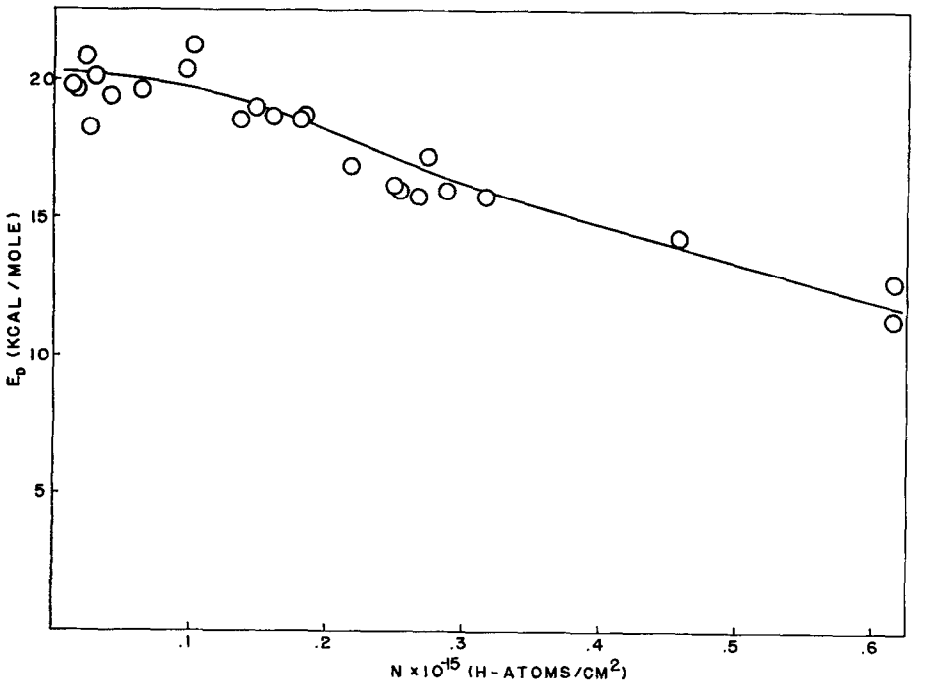

FIG. 5. Energy of activation for desorption of hydrogen from iron as a function of adsorbed amount.

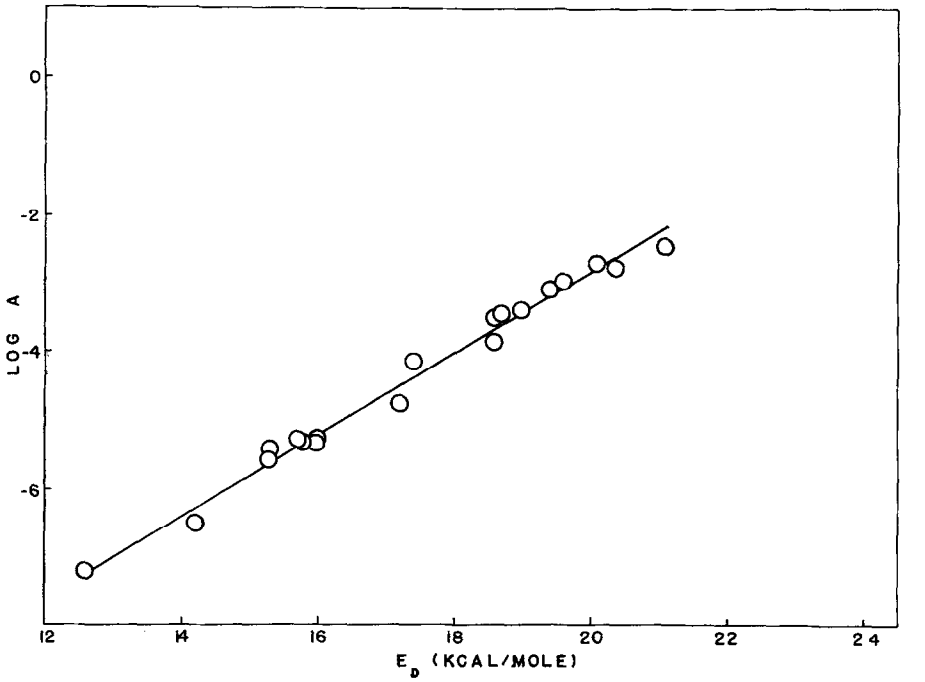

FIG. 6. Log of the preexponential factor against the activation energy for desorption of hydrogen from iron.

kinetic temperature, that temperature at which the specific rate constant has the same value regardless of the activation energy (*13*).

In the determination of the constant A_0 and T_m it must be taken into consideration that both A and E_d are, in the most general way, functions of the amount absorbed n. Thus A and E_d are not, *a priori*, independent entities. Values of A_0 and T_m calculated from the plot of Fig. 6 might then be only apparent (*14*) rather than represent a true correlation. In order to circumvent this difficulty, and following Lapujoulade (*4*) we put Arrhenius' law in the following form:

$$-\frac{dn}{dt} = An^2e^{-E_d/RT} = A_0e^{E_d/RT_m}n^2e^{-E_a/RT} \quad (3)$$

which assumes a dependence of A on E_d as expressed by Eq. (2). Equation (3) can be rearranged to:

$$-\frac{1}{n^2}\frac{dn}{dt} = A_0 \exp\left[E_d/R\left(\frac{1}{T_m} - \frac{1}{T}\right)\right] \quad (4)$$

A least squares analysis of $\log[-(1/n^2)(dn/dt)]$ against E_d/R at different temperatures ($T = T_K$, 429.7°K, 453.4°K, and 476.3°K) should be able to provide A_0 and T_m. The correlation coefficients were greater than 0.7 when this was done for the present experimental results. The resulting values were:

$$A_0 = e^{-35.33} \text{ and } T_m = 349°\text{K} \quad (5)$$

C. Equilibrium Thermodynamic Data

1. Isotherm at 298°K. Equilibrium amounts adsorbed at 298°K are shown plotted against pressure in Fig. 7. The higher pressure measurements ($>10^{-5}$ Torr) were carried out by saturation of the surface at the chosen pressure. The desorption process could not be conveniently studied at these higher pressures because the number of molecules in the measuring cell far exceeded the amount of molecules adsorbed on the specimen. Under these conditions, flashing the wire does not produce an observable deflection of the pressure recording. Therefore, after saturation, it was necessary to pump out to a pressure region ($<10^{-7}$ Torr) where the desorption peak could be observed with reasonable sensitivity. Since this pumping-

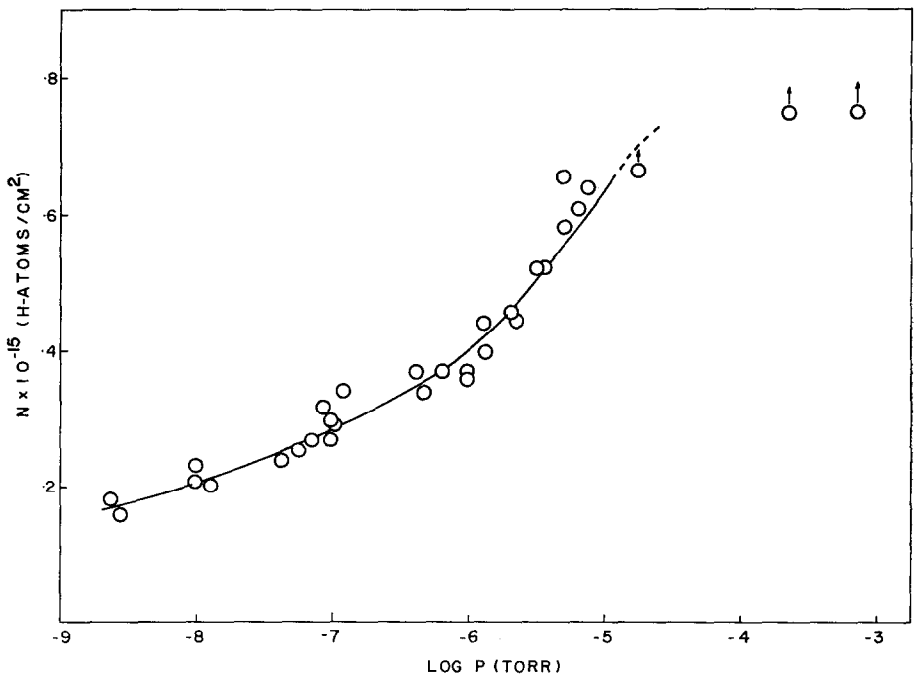

FIG. 7. Equilibrium adsorbed amounts of hydrogen on iron at 298°K, as a function of pressure.

out-time was of the order of 1 min and desorption is an activated process a substantial amount of adsorbed species was not lost during pumpdown from the lower pressures (10^{-6} Torr range). This loss could be significant, however, at the higher pressures ($\geq 10^{-5}$ Torr). For this reason the last three (high pressure) points of the isotherm, represent lower limits and most likely, they should be higher as indicated by the arrows attached to them on the graph.

2. Isobars and isosteric heats of adsorption. The isobars are shown in Fig. 8 for three different pressures. These data can be differentiated at a particular coverage to give the isosteric heat of adsorption according to the Clapeyron equation:

$$\left[\frac{\partial \ln p}{\partial(1/T)}\right]_{n=\text{constant}} = -\frac{\Delta H_{\text{isosteric}}}{R} = \frac{Q_{\text{isosteric}}}{R} \quad (6)$$

where p is pressure; T, absolute temperature; $\Delta H_{\text{isosteric}}$, the difference between the molar enthalpy of the hydrogen gas, $\bar{H}_g$, and the partial molar enthalpy of the adsorbed hydrogen, $\bar{H}_s$; and $Q_{\text{isosteric}}$, the isosteric heat of adsorption.

The isosteric heats are plotted versus coverage in Fig. 9. A comparison of Figs. 9 and 5 reveals that E_d and $(-\Delta H_{\text{isosteric}})$ are close in value (about 20 kcal mole^{-1} at low coverages) and begin to decrease at cover-

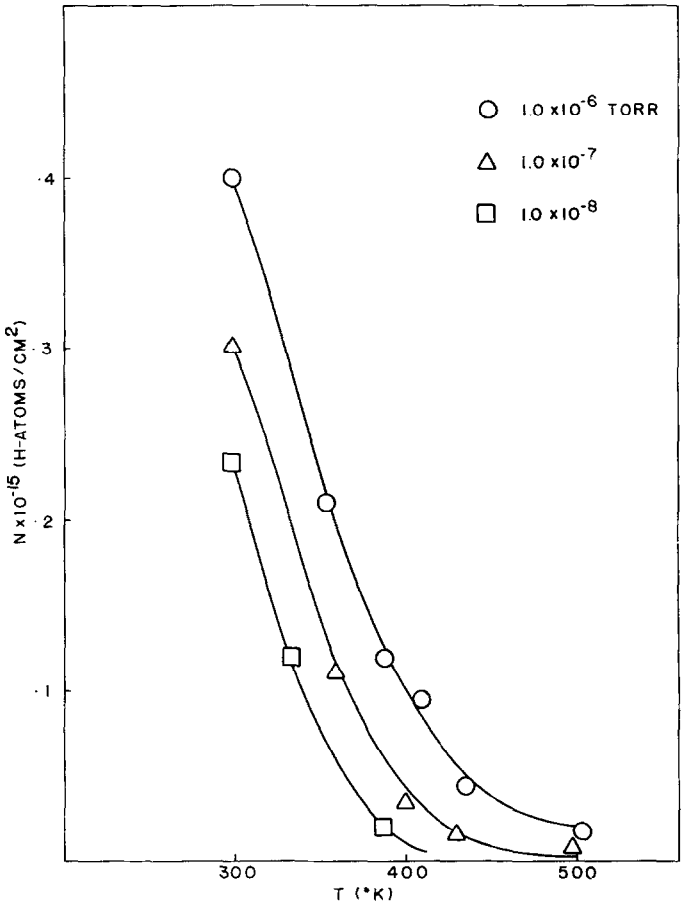

FIG. 8. Equilibrium adsorbed amounts of hydrogen on iron as a function of temperature at the indicated pressures.

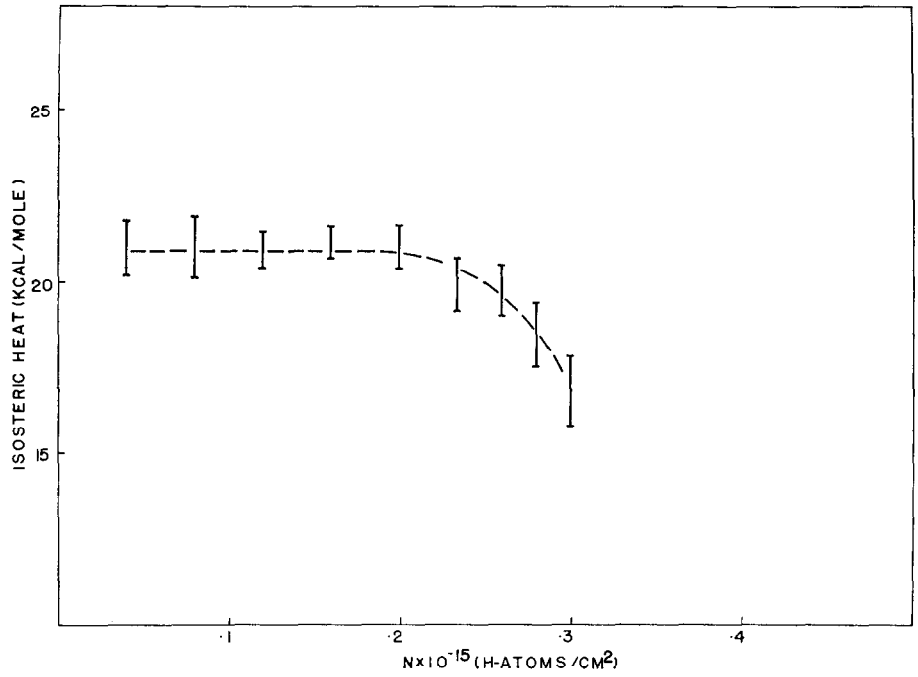

FIG. 9. Isosteric heats of adsorption of hydrogen on iron against adsorbed amount.

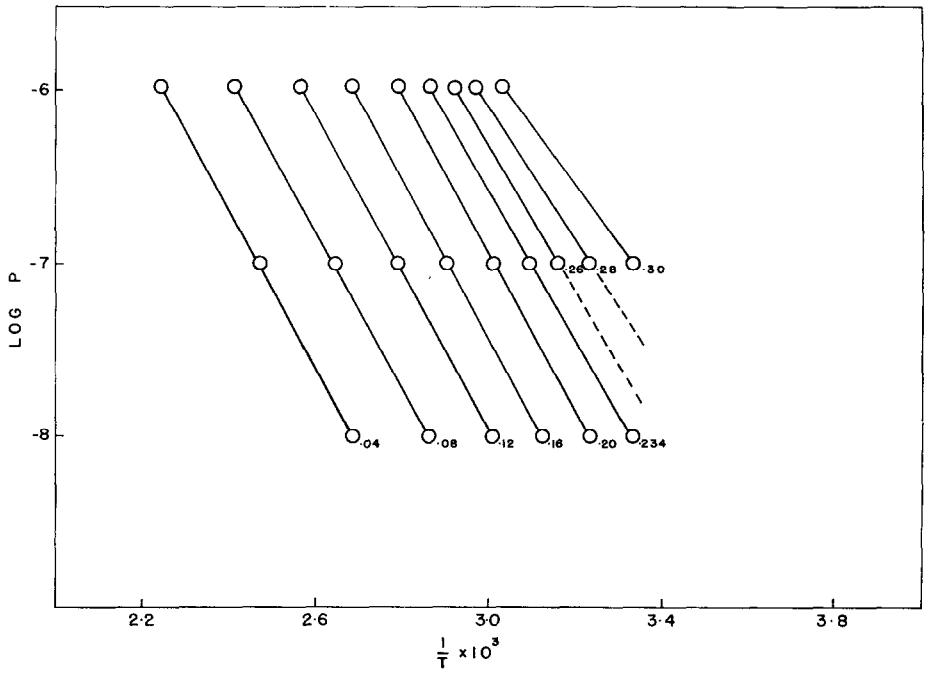

FIG. 10. Equilibrium pressure values of hydrogen on iron against $1/T$ at the indicated adsorbed amounts (units of 10^{15} H-atoms cm^{-2}).

ages larger than about 0.2×10^{15} H-atoms cm^{-2}.

3. Entropy of the adsorbed species. The procedure of Sweet and Rideal (*15*) for obtaining entropies was closely followed over the low coverage region to which our data are limited.

From the averaged values of the isobars, Fig. 8, plots of the isosteres were made and are shown in Fig. 10. Because of the averaging process, the lines of Fig. 10 are smoother than those presented in Fig. 9. The isosteric heat $(\bar{H}_g - \bar{H}_s)$ is plotted in Fig. 11, together with the molar integral heat of adsorption, $(\tilde{H}_g - \tilde{H}_s)$—obtained by planimetry from the isosteric heat using the relationship (*16*):

$$\tilde{H}_g - \tilde{H}_s = \frac{1}{\theta}\int_0^\theta (\bar{H}_g - \bar{H}_s)d\theta, \qquad (7)$$

where θ, is the coverage, defined as the ratio of the amount adsorbed to the maximum amount adsorbed at monolayer saturation (10^{15} H-atoms cm^{-2}).

The molar entropy of the adsorbed hydrogen, is computed from the relationship (*16*):

$$\tilde{S}_s = \tilde{S}_g - \frac{R}{\theta}\int_0^\theta \ln p\, d\theta - (\tilde{H}_g - \tilde{H}_s)/T, \qquad (8)$$

where $\tilde{S}_g$, the molar entropy of the hydrogen gas, in its chosen standard state (1 atm; $T = 298.96°K$) is 31.211 cal deg^{-1} $mole^{-1}$. The value of the integral in Eq. (8) was obtained by graphically integrating $\ln p$ against θ, the same information on the isotherm of Fig. 7. The molar entropy of the adsorbed hydrogen is shown in Fig. 12.

As in the case of hydrogen on nickel films studied by Sweet and Rideal (*15*) it was necessary to extrapolate the isosteres of the present work in order to obtain the molar entropy; the validity of this method as a means of calculating molar entropies is checked by comparison with the differential entropy $\bar{S}_s$ of the adsorbed hydrogen, determined directly from the individual isosteres shown as points in Fig. 12. The values of $\bar{S}_s$ were obtained by graphical differentiation of the molar entropy (continuous curve in Fig. 12) using the following relationship (*16*):

$$\bar{S}_s = \theta\frac{d\tilde{S}_s}{d\theta} + \tilde{S}_s. \qquad (9)$$

The agreement seems to be satisfactory since the differential entropy is very sensitive to any error in the isosteric heat from which the entropy is calculated.

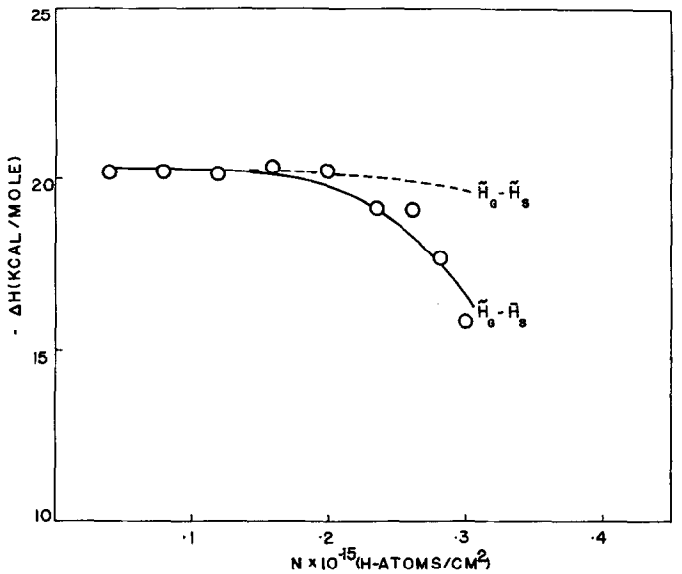

FIG. 11. Differential $(\bar{H}_g - \bar{H}_s)$ and integral $(\tilde{H}_g - \tilde{H}_s)$ heat of adsorption of hydrogen on iron against adsorbed amount in the same temperature range of Figs. 4–10.

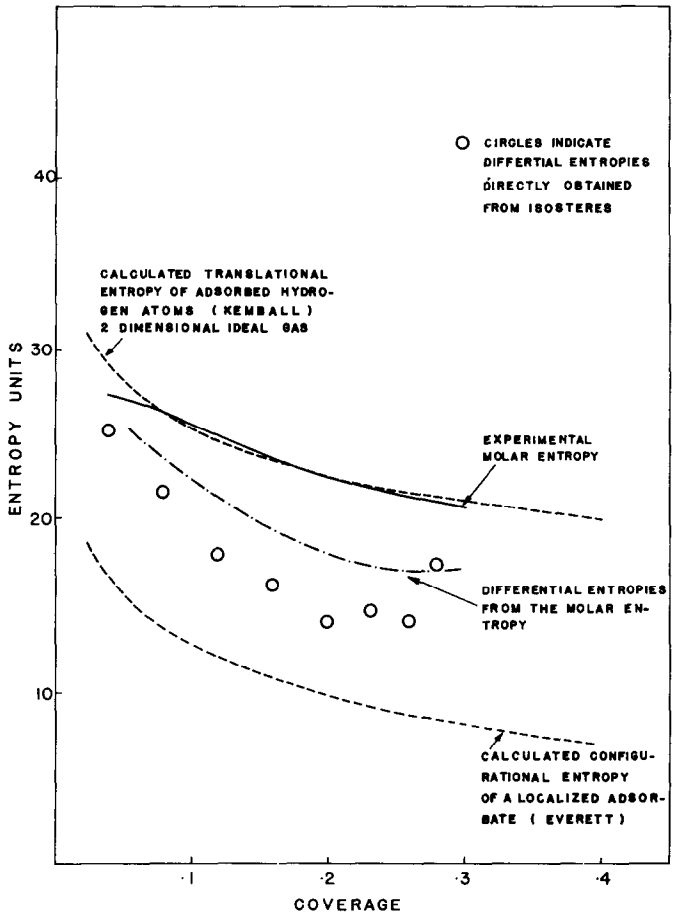

FIG. 12. Molar entropies and differential molar entropies of hydrogen on iron against coverage, considering 10^{15} H-atoms cm^{-2} as unity coverage. Entropy units are (cal deg^{-1}).

D. Rates of Adsorption

By varying the exposure time of the specimen at different hydrogen pressures, information on the amount adsorbed as a function of time is obtained by using the material balance relationships. Figure 13 presents some of these experimental results. Since the specimen was kept hot (at about 800°C in these experiments) prior to the initiation of an adsorption cycle, and since it takes a finite time for the specimen to cool to the adsorption equilibrium temperature of about 300°K (note the evolving profile in Fig. 13), a corresponding temperature effect appears in the initial portion of these curves. The process can be formulated by:

$$\frac{dn}{dt} = V_a - V_d \tag{10}$$

where V_a and V_d are rates of adsorption and desorption, respectively, and n is the amount adsorbed (molecules cm^{-2}).

Since the analysis of the desorption rates gives a complete expression for V_d [Eq. (1)], whose constants A, the preexponential factor, and E_d, activation energy for desorption, are determined experimentally (Sec. III.B), it is then straightfoward to arrive at $V_a = V_a(t)$ from Eq. (10).

The rate of adsorption V_a can be expressed most generally as:

$$V_a = V_a(p, n, T), \tag{11}$$

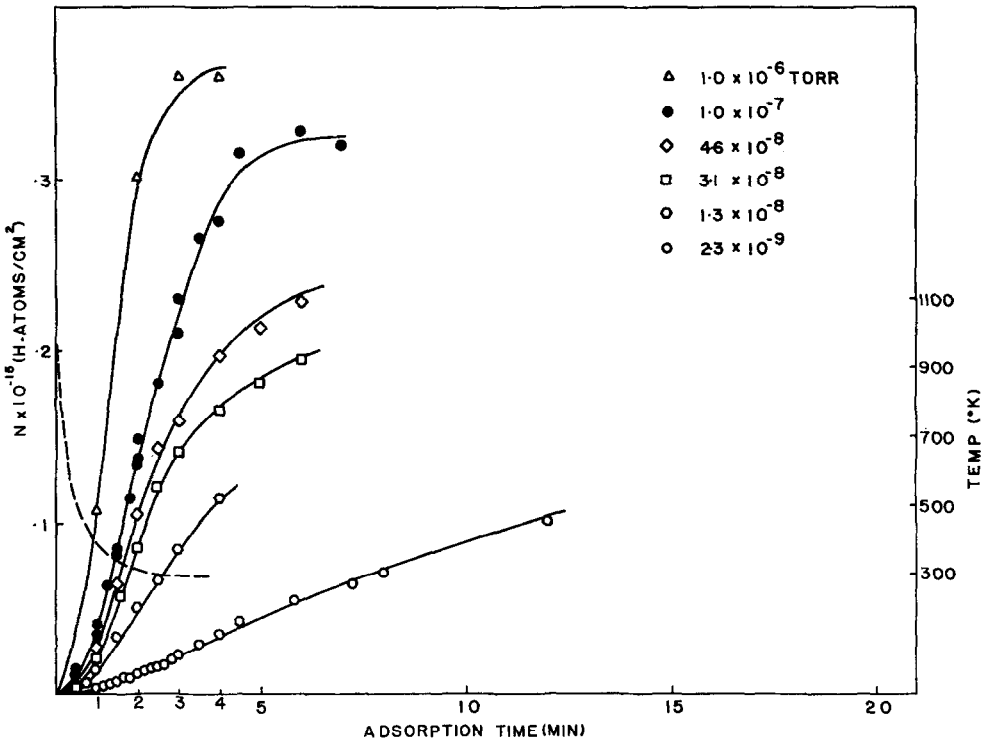

FIG. 13. Kinetics of hydrogen adsorption on iron at 298°K (—); the temperature cooling profile of the sample (- -).

where p is pressure; n is amount adsorbed; and T is temperature.

From theoretical considerations (*17*, *18*), and also in conformity with general experimental results (*19*) the functional dependence of V_a on p, n and T is usually written:

$$V_a = K_a p^{\alpha} f(n) e^{-E_a(n)/RT} \qquad (12)$$

where E_a is the activation energy for adsorption and K_a is a constant.

A plot of log V_a against log p will determine the value of α. This is shown in Fig. 14, where the straight line drawn through the data points has a slope of $\alpha = 1$.

From Eq. (12) and with $\alpha = 1$ the sticking coefficient σ is defined as:

$$\sigma = \frac{V_a}{Z} = K_a f(n) e^{-E_a(n)/RT} (2\pi mkT)^{1/2}, \quad (13)$$

where $Z = p/(2\pi mkT)^{1/2}$ is the number of collisions per square centimeter sec.

Figure 15 shows a plot of log σ against the amount adsorbed, at room temperature. The initial value, extrapolated to zero coverage, falls around 0.05. This result is important because it reflects upon the mechanism of adsorption.

IV. Discussion

A. *Changes of Adsorbed Amount During Cleaning Treatment*

The following observations can be made:

Adsorbed amounts were invariably lower (20 to 60%) on the reduced surfaces (subject to hydrogen treatment only) than surfaces that had been reduced and ion bombarded.

Argon bombardment resulted in poisoning of the surface when carbon monoxide was present even at residual partial pressures as low as 10^{-8} Torr.

Degassing of the gauges and/or bakeout of the system, contaminated the specimen but a new bombardment cycle restored the full adsorption capacity.

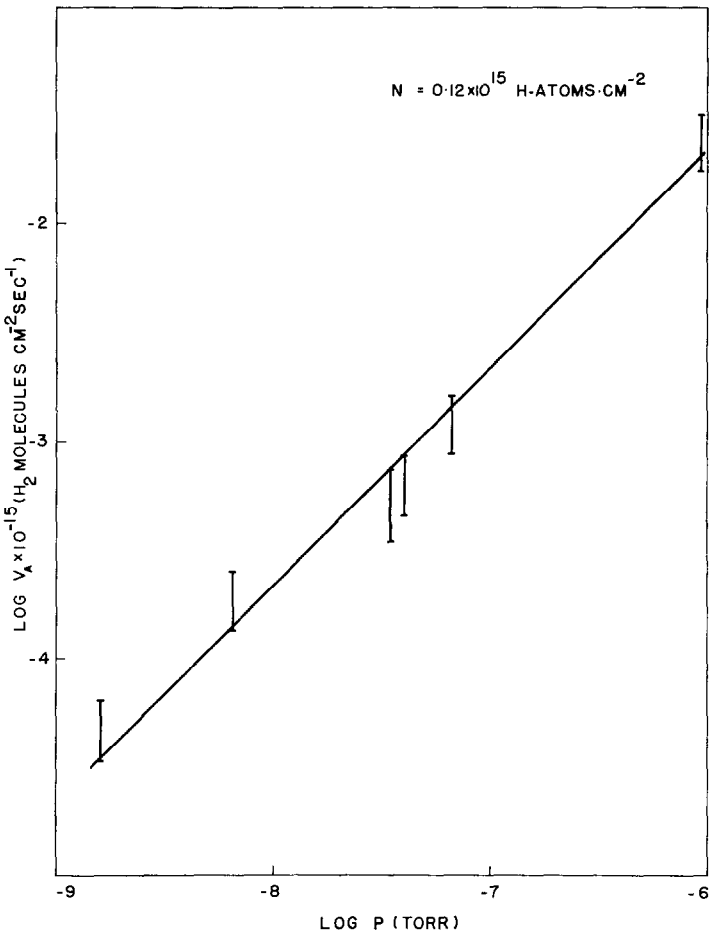

FIG. 14. Adsorption rates of hydrogen on iron as a function of pressure.

B. Desorption Cycle

1. Adsorbed phases at 298°K. At exposure times of less than 30 min only one adsorbed phase is found. The appearance of a second peak upon flash after long exposure times is probably due to slow diffusion of hydrogen atoms from inside the bulk. Other interpretations of this second peak are possible, of course but, based on the clear exposure-time dependence, we interpret results in terms of a single adsorbed phase throughout this paper. No further tests were made to prove or contradict this suggestion.

2. Reaction order. The fact that desorption is a second order reaction suggests that the adsorbed species are hydrogen atoms; i.e., adsorption proceeds with dissociation at room temperature.

3. Desorption rates. The activation energies for desorption presented in Fig. 5 represent average energies of the adsorbed population. The shape of the curve agrees well with the general relationship of the binding energy of an adsorbed layer when nearest neighbor interactions are important (*20*). Because of the small size of the hydrogen atom, this interaction can be visualized taking place through the electron cloud of the metal.

The data plotted in Fig. 6, show that the preexponential factor A of the desorption rate constant can be correlated with the activation energy for desorption E_d according to a typical "compensation law."

This effect is well documented experimentally in heterogeneous catalysis (*21*). Con-

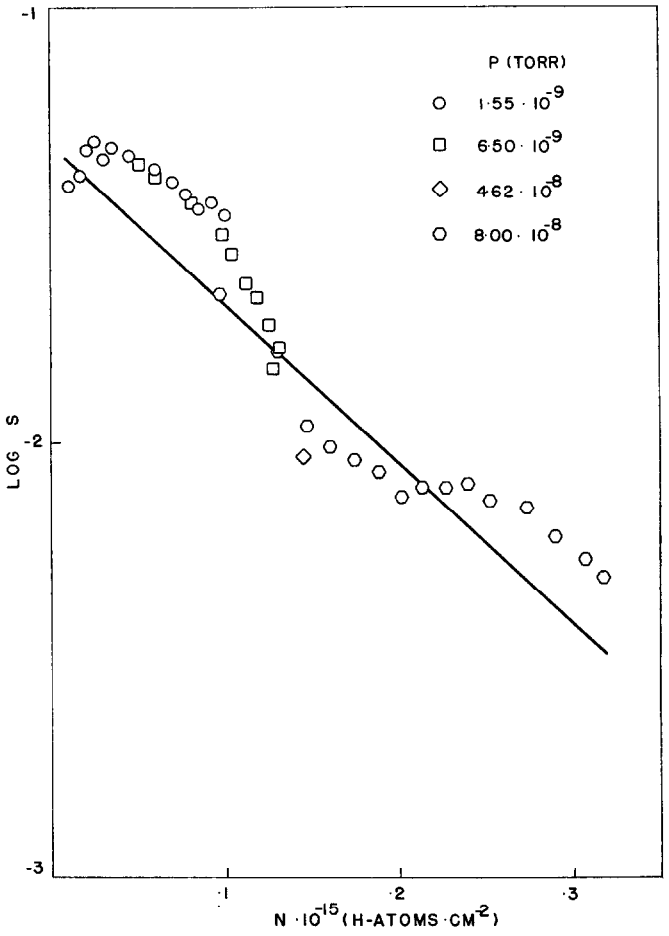

FIG. 15. Sticking coefficient of hydrogen on iron as a function of absorbent amount.

stable (*22*) and Cremer (*13*) formulated the hypothesis of heterogeneity of the surface as a possible explanation of the compensation effect. In the case of desorption from a metal surface Degras (*12*) observed a similar compensation law when studying the desorption of CO from nickel single crystals but he concluded that heterogeneity of the surface could not explain the observed results. This was supported by Armand and Lapujoulade (*21*) who showed, in a theoretical treatment of first order desorption reactions, that a heterogeneous surface could not explain the compensation law for desorption reactions on metals. In the present study (*11*, *23*) we have found that the observed effect is compatible with a homogeneous surface and a mobile adsorbate whose desorption rate is affected by changes in the activity coefficients of the adsorbed species induced by strong lateral interactions.

C. Equilibrium Data

1. Isotherm at 298°K. At low coverages, the isotherm is of the Freundlich type ($\theta = \beta p^{1/\gamma}$, where θ is the coverage, p the pressure and β and γ are constants) as can be seen from the log θ against log p plot of Fig. 16 (θ's in Fig. 16 are average values of data from Fig. 7). Deviation from Freundlich behavior at increasing coverages would indicate a dependence of γ on the adsorbed amount. Rideal (*16*) has derived the Freundlich isotherm considering a two-dimensional layer which obeys an equation of state $\Phi\sigma = nRT$ (where Φ is the spreading

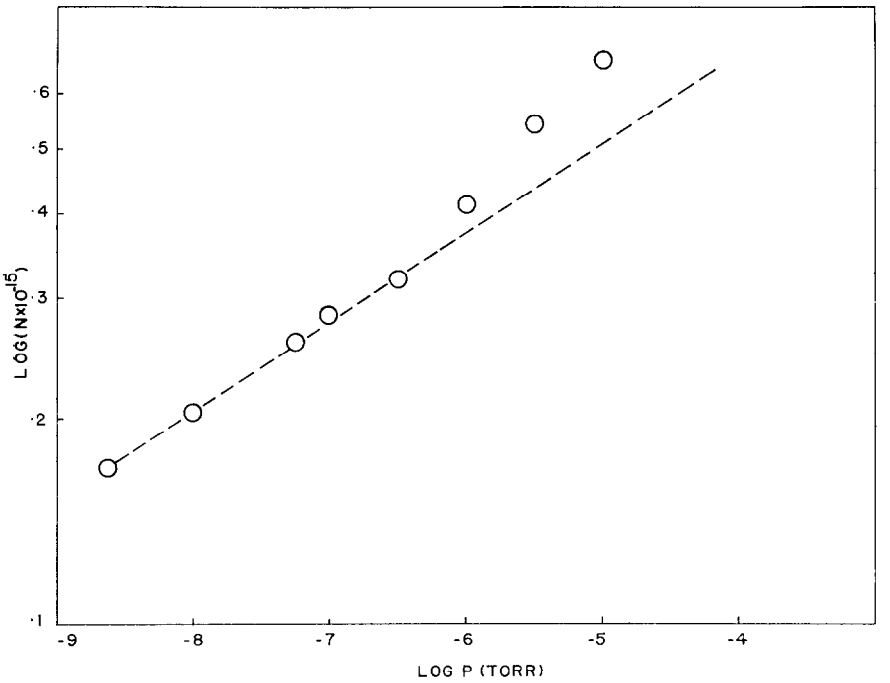

FIG. 16. Plots of the average equilibrium adsorbed amounts of hydrogen on iron (log scale) at 298°K, as a function of log pressure.

pressure and ω is the molar area of the absorbate), allowing, in addition, for interactions between adsorbed species. Conformity to the Freundlich isotherm is not conclusive evidence of lateral interactions, however, since Zeldowitch (*24*) and Halsey and Taylor (*25*) have also derived this isotherm based only in a heterogeneous site distribution in which the sites differ from one another solely in the adsorption energy and not at all in entropy. Furthermore, it was necessary to assume that the sites had an exponential distribution of adsorption energies. Our experimental activation energies of desorption (Fig. 5) (which to a close approximation are the adsorption energies) indicate a trend different than exponential. Instead, they agree with a general expression for the variation of adsorption energy E with coverage θ for a mobile adsorbate, which is given by Fowler and Guggenheim (*20*) as:

$$E = E_0 - W(\theta - f(\theta)), \qquad (14)$$

where E_0 is the adsorption energy with no interaction and W is a characteristic energy parameter of the adsorbate only.

According to this expression, at low θ, E is either constant or varies linearly with coverage. The Fowler and Guggenheim treatment takes into account nearest neighbor interactions which could also be responsible for the Freundlich type isotherm as shown by Rideal (*16*) as mentioned above. The form of the isotherm and the dependence of adsorption energy on coverage suggests a mobile adsorbate. By combining this idea with the reaction order discussed in Sec. B.2, we envision this substrate as a two-dimensional gas of hydrogen atoms.

2. Isosteric heats of adsorption. The agreement in magnitude between the activation energies (Fig. 5) and the isosteric heats (Fig. 9) is significant. This agreement lends weight to the desorption analysis and suggests a small (or zero) activation energy for adsorption.

The chemisorption heats obtained in the present work are compared in Fig. 17 with published calorimetric results (*26–28*). These latter results, as do most of the work concerning evaporated films, suffer from the absence of a precise definition of a mono-

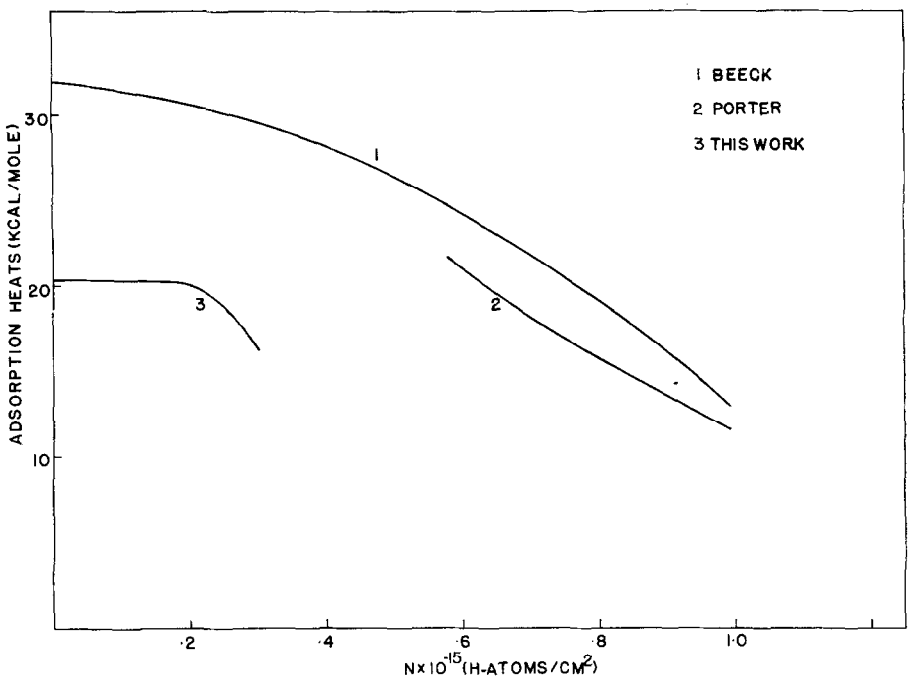

FIG. 17. Adsorption heats of hydrogen on iron against adsorbed amount at 298°K.

layer. Beeck (*27*) took $\theta = 1$ as the amount adsorbed in equilibrium with a pressure of 0.1 mm Hg, the point where saturation seemed to occur. Based on the present results, this choice was rather fortunate since our isotherm will probably level off at 10^{-1} Torr with a coverage of about 10^{15} H-atoms cm^{-2}. This choice enables a comparison with the results of others. Porter and Tompkins (*29*) reported heats calculated from equilibrium data in the range of 10^{-5} to 1 Torr. Since at 10^{-5}, in our isotherm, $\theta = 0.675$, their data are plotted from this point on. The important observation is that our values are much lower than those obtained from evaporated films. Rather than attribute this difference to contamination of the films we prefer to think it is due to a roughness effect (*30*).

3. Entropy of the adsorbed species. In order to interpret the molar entropy found in this work, it is necessary to compare it with entropies of certain possible modes of adsorption, namely the extreme cases of localized and mobile adsorbates.

Everett (*31*) has shown that the molar configurational entropy $\tilde{S}_{sc}$ of a localized adsorbed layer when adsorption is accompanied by dissociation, is given by:

$$\tilde{S}_{sc} = -2R \ln \theta - 2R(1 - \theta)/\theta \ln(1 - \theta) \text{ cal deg}^{-1} \text{ mole}^{-1}. \quad (15)$$

The translational molar entropy of a two-dimensional gas has been shown by Kemball (*32*) to be:

$$\tilde{S}_{2T} = R \ln MT\mathscr{a} + 65.8 \text{ cal deg}^{-1} \text{ mole}^{-1} \quad (16)$$

where R is the gas constant, M the molecular weight of the adsorbed species and $\mathscr{a}$ is the area (cm^2) available for a molecule on the surface in the standard state. Furthermore, we have considered that at unity coverage the amount adsorbed is 10^{15} H-atoms cm^{-2}.

The important conclusion from Fig. 12, is that our adsorbate behaves as a mobile two-dimensional gas even at coverages as low as 0.05. In the very early stages, $\theta < 0.05$, the trend points to less mobile behavior and in fact, we could expect heterogeneities to play a role at these very low coverages. We would also expect that at high coverages, the molar entropy will depart from the ideal two-dimensional values and approach a

more restricted type of mobility due to the repulsive forces between the adsorbed species.

Comparing our results on iron with those obtained by Sweet and Rideal (*15*) on evaporated nickel films, it is quite striking that their adsorbate was localized up to a coverage of about 0.4, whereas ours behaves as an ideal mobile film at a coverage as low as about 0.05. This difference is consistent with the argument that well-annealed surfaces are indeed much smoother and behave more homogeneously than evaporated films even if they have been sintered to reduce their roughness. It can be argued that the lower population of heterogeneities in well-annealed surfaces are satisfied by fewer adsorbed entities (lower coverages), whereafter, succeeding molecules adsorbed are less tightly bound and free to translate on the surface.

D. Adsorption Rates

An important problem in the study of reaction rates is the determination of the structure of the activated complex (*31*). As pointed out in Sect. III.B.2 the desorption process of the present investigation proceeds with association. This would suggest a molecular configuration for the activated complex and is consistent with Eq. (12) and linear pressure dependence for the rate of adsorption. With this choice of activated complex, the adsorption reaction can be formulated as:

$$H_2(g) \overset{K_a}{\rightleftarrows} H \cdots H \overset{kT/h}{\longrightarrow} 2H_{ads} \qquad (17)$$

and from the transition state theory:

$$V_a = \frac{kT}{h} C^{\ddagger} = \frac{kT}{h} K_a p_{H_2} \qquad (18)$$

where $C^{\ddagger}$, concentration, has replaced $a^{\ddagger}$, the activity of the activated complex, since we are considering the initial stages of adsorption where indeed $a^{\ddagger} \simeq C^{\ddagger}$.

From our study of the desorption rates we know that the activated complex possesses less entropy that the adsorbed species (log A for desorption, is always negative). Since at low coverages these are mobile, our complex should be either less mobile or immobile. Accordingly, interpretation of the sticking coefficient values can be facilitated by considering two alternative possibilities: an immobile complex and a mobile complex.

1. Immobile complex. The expression for the initial sticking probability is (*19*):

$$\sigma_0 = C_{s2} \frac{h^2}{2\pi mkT} \frac{b_{\ddagger}}{b_g} e^{-E_0/RT} \qquad (19)$$

where C_{s2} is the concentration of dual sites; $b_{\ddagger}$ contains the vibrational partition function of the activated complex; b_g is the product of the rotational and vibrational partition functions of hydrogen gas; E_0 is the difference between the zero point energies, at the absolute zero, of the activated complex and the reactants (gas molecules) which is related to the activation energy E_a by: $E_a = RT + E_0$, and the other constants have the usual meanings.

With $C_{s2} = 10^{15}$ cm^{-2}, number of nearest neighbors equal to four (most common value), $T = 298$°K, and $b_g = 3.5$ [its value for hydrogen (*20*)], values of σ_0 range from 3×10^{-2} (case of high frequencies of vibration) to much higher values for weaker vibrations ($\sigma_0 = 0.15$ for 10^{12} sec^{-1}). Laidler (*33*) points out that $b_{\ddagger}$ is very close to unity at ordinary temperatures. Such a statement would mean that the immobility of the activated complex results in too low values of the sticking coefficients ($\sim$0.03).

2. Mobile complex. A second mechanism consists of a gaseous molecule entering the adsorbate (or placing itself just above it), whereupon it loses one degree of rotational freedom (rotation at right angles to the surface), but still retains two degrees of translational (freedom of movement in the plane of the surface). The expression for the reaction rate does not involve the concentration of adsorption sites since they are not reactants, and the following relationship holds (*19*):

$$\sigma_0 = \left(\frac{h^2}{8\pi^2 IkT}\right)^{1/2} e^{-E_0/RT} \qquad (20)$$

where I is the moment of inertia of the hydrogen molecule. In this case, if no activation energy is present, $\sigma_0 = 0.52$. Therefore, the loss of one degree of rotation does not fully account, by itself, for the low initial sticking coefficient observed (0.05).

In order to see whether a small activation energy is required for adsorption we investigated possible temperature dependence of the adsorption rates. To do this, the kinetic data of Fig. 13 were examined at low coverages (0.02 and 0.04 $\times$ 10^{15} H-atoms cm^{-2}), that is, the region where the sample is cooling off. The results are shown in Fig. 18. Although the scattering of the data points does not suggest a precise linear correlation between log σ and $1/T$ the trend does indicate a small energy of activation associated with the adsorption process.

If we accept mechanism II as responsible for adsorption, which means a mobile complex of restricted rotational freedom, an activation energy of about 0.5 kcal $mole^{-1}$ would account for the low sticking coefficients found. This is consistent with the results shown in Fig. 18.

This mechanism is supported by a comparison of the amount adsorbed at 100°K with that adsorbed at higher temperatures. The resulting normalized isobar is shown in Fig. 19. The upper data point at 100°K corresponds to the amount adsorbed after the sample has been saturated with hydrogen at room temperature and then cooled to 100°K, whereas the lower points, at 100°K, are obtained with the specimen cooled before admission of hydrogen. This result is similar to the one observed by Ponec, Knor and Cerny (7) using evaporated films. The lower branch indicates that a small energy of activation is needed for chemisorption. The upper branch, interpreted by Ponec, Knor and Cerny (7) as adsorption on sites of lower adsorption energies, can also be interpreted as a different mode of adsorption, molecular hydrogen, occurring at lower temperatures, and then it is not necessarily a consequence of heterogeneity.

V. Conclusions

This study has brought out a certain number of features of the hydrogen–iron system:

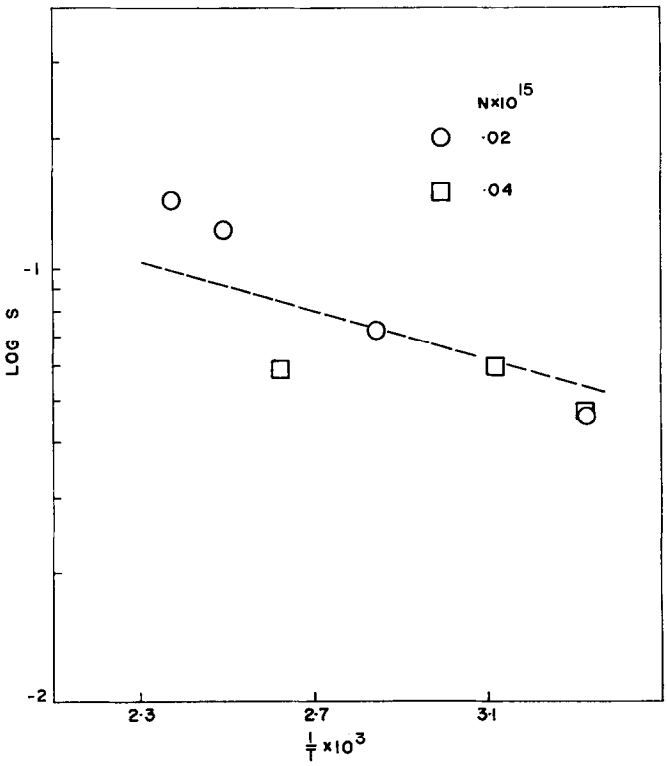

Fig. 18. Sticking probability (log scale) of hydrogen on iron against $1/T$.

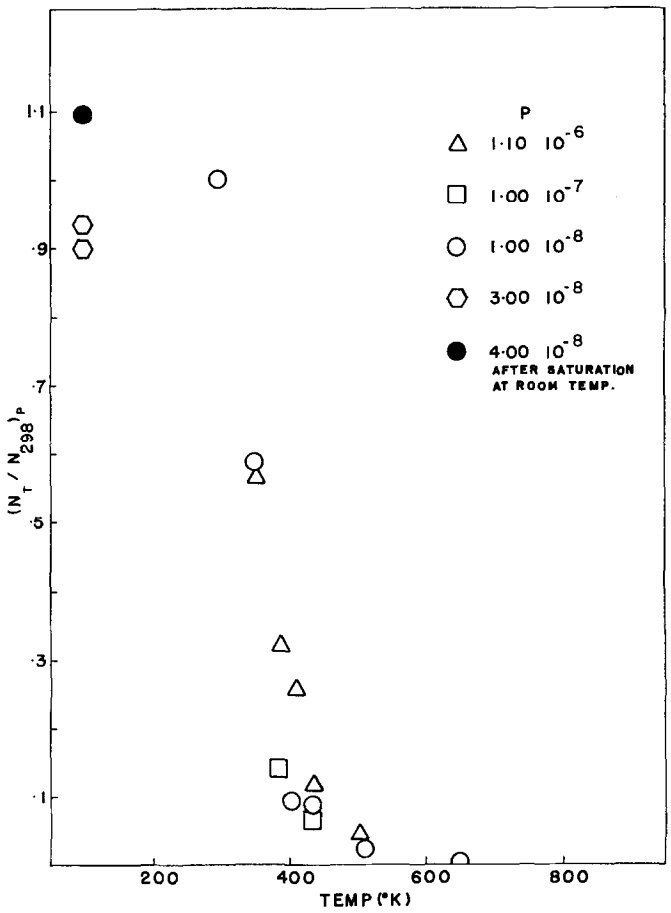

FIG. 19. Ratio of the adsorbed amounts of hydrogen on iron at temperature T and at 298°K, as a function of T.

Argon ion bombardment, together with extensive annealing, under carefully controlled UHV conditions, is a convenient method of surface preparation of ion, judging from the adsorbed amounts found. The presence of CO (even at 10^{-8} Torr) heavily contaminates the surface during bombardment.

The desorption process is second order. It involves a collision of two adsorbed hydrogen atoms followed by departure of hydrogen molecules from the surface.

The activation energy of desorption is constant at low coverage (20.3 kcal mole^{-1}) and begins to decrease when a coverage of about 0.2×10^{15} H-atoms cm^{-2} has been reached. This result can be interpreted as a consequence of adsorbate–adsorbate interactions, which is consistent with the shape of the isotherm at 298°K.

The experimental results display a compensation relationship between the preexponential factor and the activation energy for desorption. Such an effect is compatible with a mobile adsorbate, which displays nonideal behavior caused by strong lateral interactions at increasing coverages. Such behavior can be taken into account by the introduction of activity coefficients.

The heats of adsorption found in the present work are lower than those reported for evaporated films. This disagreement can be explained as resulting from the relatively high roughness of the evaporated films as compared to the smoother, more coherent surfaces of the filaments used in the present investigation.

Entropy calculations indicate that the adsorbate is indeed mobile and that its be-

havior at low coverages approaches that of an ideal two-dimensional gas.

The initial rates of adsorption are well explained by assuming that the activated complex is molecular in nature, but has lost rotational freedom with respect to the gas phase and requires about 0.5 kcal mole^{-1} to be formed.

Acknowledgments

The authors express their appreciation to K. Klier and H. Leidheiser, Jr., for stimulating discussions. Financial support from the Center for Surface and Coatings Research, under a Department of Defense, Office of Naval Operations, contract No. 0014-67-A-0370-0006 is gratefully acknowledged.

References

1. Ehrlich, G., *in* "Advances in Catalysis" (D. D. Eley, H. Pines and P. B. Weisz, eds.), Vol. 14, p. 255. Academic Press, New York, 1963.
2. Mimeault, V. J., and Hansen, R. S., *J. Chem. Phys.* **45**, 2240 (1966); Bergsnov-Hansen, B., and Pasternak, R. A., *Surface Sci.* **17**, 402 (1969) and literature cited therein.
3. Adams, D. L., and Germer, L. H., *Surface Sci.* **23**, 419 (1970).
4. Lapujoulade, J., *Nuovo Cimento, Suppl.* **5**, 433 (1967).
5. Gasser, R. P. H., Roberts, K., and Stevens, A. J., *Trans. Faraday Soc.* **65**, 3105 (1969).
6. Bond, G. C., *Surface Sci.* **18**, 11 (1969).
7. Ponec, V., Knor, Z., and Cerny, S., *Discuss. Faraday Soc.* **41**, 149 (1966).
8. Liang, I. C., *Can. J. Chem.* **33**, 279 (1955).
9. Farnsworth, H. E., Schlier, R. E., George, T. H., and Burger, R. M., *J. Appl. Phys.* **29**, 1150 (1958).
10. Chornet, E., Coughlin, R. W., and Leidheiser, H., Jr., presented: Nat. Colloid Surface Chem. Symp., 44th, Bethlehem, PA, June, 1970.
11. Chornet, E., PhD dissertation, Lehigh Univ., 1971.
12. Degras, D. A., *C. R. Acad. Sci., Ser. C* **262**, 1737 (1966).
13. Cremer, E., *in* "Advances in Catalysis" (W. G. Frankenburg, V. I. Komarewsky and E. K. Rideal, eds.), Vol. 7, p. 75. Academic Press, New York, 1955.
14. Exner, O., *Collect. Czech. Chem. Commun.* **29**, 1094 (1964).
15. Sweet, F., and Rideal, E. K., *Actes Congr. Int. Catal., 2nd, 1960*, 175 (1961).
16. Rideal, E. K., "Surface Chemistry." Cambridge Univ. Press, London, 1930.
17. Parlin, R. B., Wallestein, M. G., Zwolinski, B. J., and Eyring, H., *in* "Catalysis" (P. H. Emmett, ed.), Vol. 2, Chap. 5. Reinhold, New York, 1955.
18. Glasstone, S., Laidler, K. J., and Eyring, H., "Theory of Rate Processes." McGraw-Hill, New York, 1941.
19. See for instance Hayward, D. O., and Trapnell, B. M. W., "Chemisorption." Butterworths, London, 1964; or Bond, G. C., "Catalysis by Metals." Academic Press, New York, 1961.
20. Fowler, R. H., and Guggenheim, E. A., "Statistical Thermodynamics," p. 441. Cambridge Univ. Press, London, 1949.
21. Armand, G., and Lapujoulade, J., *Surface Sci.* **6**, 345 (1967).
22. Constable, F. H., *Proc. Roy. Soc., Ser. A* **108**, 355 (1925).
23. Chornet, E., and Coughlin, R. W., unpublished data.
24. Zeldowitch, J., *Acta Physizochim. URSS*, **1**, 961 (1935).
25. Halsey, G. D., and Taylor, H. S., *J. Chem. Phys.* **15**, 624 (1947).
26. Beeck, O., Cole, W. A., and Wheeler, A., *Discuss. Faraday Soc.* **8**, 314 (1950).
27. Beeck, O., in "Advances in Catalysis" (W. G. Frankenburg, V. I. Komarewsky and E. K. Rideal, eds.), Vol. 2, p. 151. Academic Press, New York, 1951.
28. Ponec, V., and Knor, Z., *J. Catal.* **10**, 73 (1968); general bibliography on heats.
29. Porter, A. C., and Tompkins, T. C., *Proc. Roy. Soc., Ser. A* **217**, 574 (1953).
30. Klier, K., Zettlemoyer, A. C., and Leidheiser, H., Jr., *J. Chem. Phys.* **52**, 2, 601 (1970).
31. Everett, D. H., *Proc. Chem. Soc., London* 38, (1957).
32. Kemball, C., *Proc. Roy. Soc., Ser. A* **187**, 73 (1946).
33. Laidler, K. J., *in* "Catalysis" (P. H. Emmett, ed.), Vol. 1, pp. 195, 200. Reinhold, New York, 1954.